Scripta Materialia 157 (2018) 6–9

Contents lists available at ScienceDirect

Scripta Materialia

journal homepage: www.elsevier.com/locate/scriptamat

Regular article

Ductile and intergranular brittle fracture in a two-step quenching and partitioning steel

Zhiping Xiong [a,*], Pascal J. Jacques [a], Astrid Perlade [b], Thomas Pardoen [a]

[a] Université catholique de Louvain, Institute of Mechanics, Materials and Civil Engineering, IMAP, 1348 Louvain-la-Neuve, Belgium
[b] ArcelorMittal Global R&D Maizières Products, Voie Romaine, BP 30320, 57283 Maizières-lès-Metz Cedex, France

ARTICLE INFO

Article history:
Received 9 June 2018
Received in revised form 18 July 2018
Accepted 22 July 2018
Available online xxxx

Keywords:
Quenching and partitioning
Ductile fracture
Brittle fracture
Double edge notched tension

ABSTRACT

A two-step quenching and partitioning steel exhibits ductile fracture under uniaxial tension and unexpectedly intergranular brittle fracture in the case of pre-cracked configuration. A gradual retained austenite-to-martensite transformation because of low stress triaxiality under uniaxial tension, leads to ductile fracture with voids formation between fresh and tempered martensite resulting from the large strain partitioning and localization. When the retained austenite fast transforms to martensite in the near crack tip region because of high stress triaxiality, intergranular fracture is promoted by the high maximum principal stress level and by the formation of brittle martensite necklace along tempered martensitic packet boundaries.

Advanced high strength steels (AHSSs) result from the continuous up-to-date requirements of safety, weight reduction and cost saving active in the automotive industry. Following first and second generation AHSSs, quenching and partitioning (Q & P) steels, as third generation AHSSs, were first reported by Speer et al. [1]. From then on, the effect of alloying elements, quenching temperature and holding time at different partitioning temperatures on microstructure and mechanical properties has been intensively studied [2–6]. The microstructure components of Q & P steels evolving with quenching temperature can be appropriately evaluated based on Koistinen–Marburger relationship [7]. This assumes that full carbon partitioning between martensitic laths and austenite has been reached prior to quenching to room temperature. Based on the experiments following this model, the largest amount of retained austenite (RA) can be found at a well-defined quenching temperature, normally associated to the best product of ultimate tensile strength and total elongation [5,6].

Although the product of ultimate tensile strength and total elongation has been widely used as an indicator for the steel performance, Casellas et al. [8] and Hisker et al. [9] demonstrated that the cracking process observed in cut edges of some AHSSs used by the automotive industry could not be rationalized by this parameter. This effect is related to the stress state generated at the tip of a sharp defect, involving a relative high local stress triaxiality. Only fracture mechanics based approach is thus appropriate to address this issue. The double edge notched tension (DENT) specimen constitutes a particularly suitable geometry due to its symmetry and the absence of bending component [10]. In this study, the fracture mechanisms occurring in a Q & P steel have been assessed using uniaxial tension and DENT tests. The transformation rate of RA-to-martensite plays an important role in the control of the fracture mechanisms.

The chemical composition of studied steel is 0.3 C–2.5 Mn–1.5 Si–0.8 Cr (wt%). DENT samples ($100 \times 50 \times 3$ mm^3) and uniaxial tensile samples (3 mm of thickness, 6 mm of width and 26 mm of gauge length) were machined along the rolling direction of hot and cold rolled plates. Samples were heated up to 900 °C and held at this temperature for 160 s using a fluidized bed furnace, quenched to 220 °C using a salt bath furnace, heated up to 400 °C and held at this temperature for 500 s in another salt bath furnace and finally water quenched. The microstructure consists of 18.2% RA (having a carbon content of 0.91 wt%, measured by X-ray diffraction), tempered martensite, and probably a small amount of untempered martensite and bainite (which have been respectively demonstrated by electron backscatter diffraction [4] and in-situ high energy X-ray diffraction [11]). After heat treatment, notches of 20 mm in length were carried out by electrical discharge machining followed by razor blade sharpening on both sides. Tensile testing of the DENT and uniaxial specimens were carried out using a screw driven universal testing machine at a cross-head speed of 1 mm/min. Fresh martensite transformed from RA was revealed by tempering at 200 °C for 2 h [12]. The microstructure etched by 2 vol% nital and fracture surface were characterized using scanning electron microscope (SEM).

Fig. 1(a, b) shows the engineering and true stress–true strain curves, as well as the variation of the incremental strain hardening exponent of the investigated steel. Due to continuous transformation of RA into martensite during uniaxial tension (which was demonstrated for other steel

* Corresponding author.
E-mail address: zhiping.xiong@uclouvain.be (Z. Xiong).

https://doi.org/10.1016/j.scriptamat.2018.07.030
1359-6462/

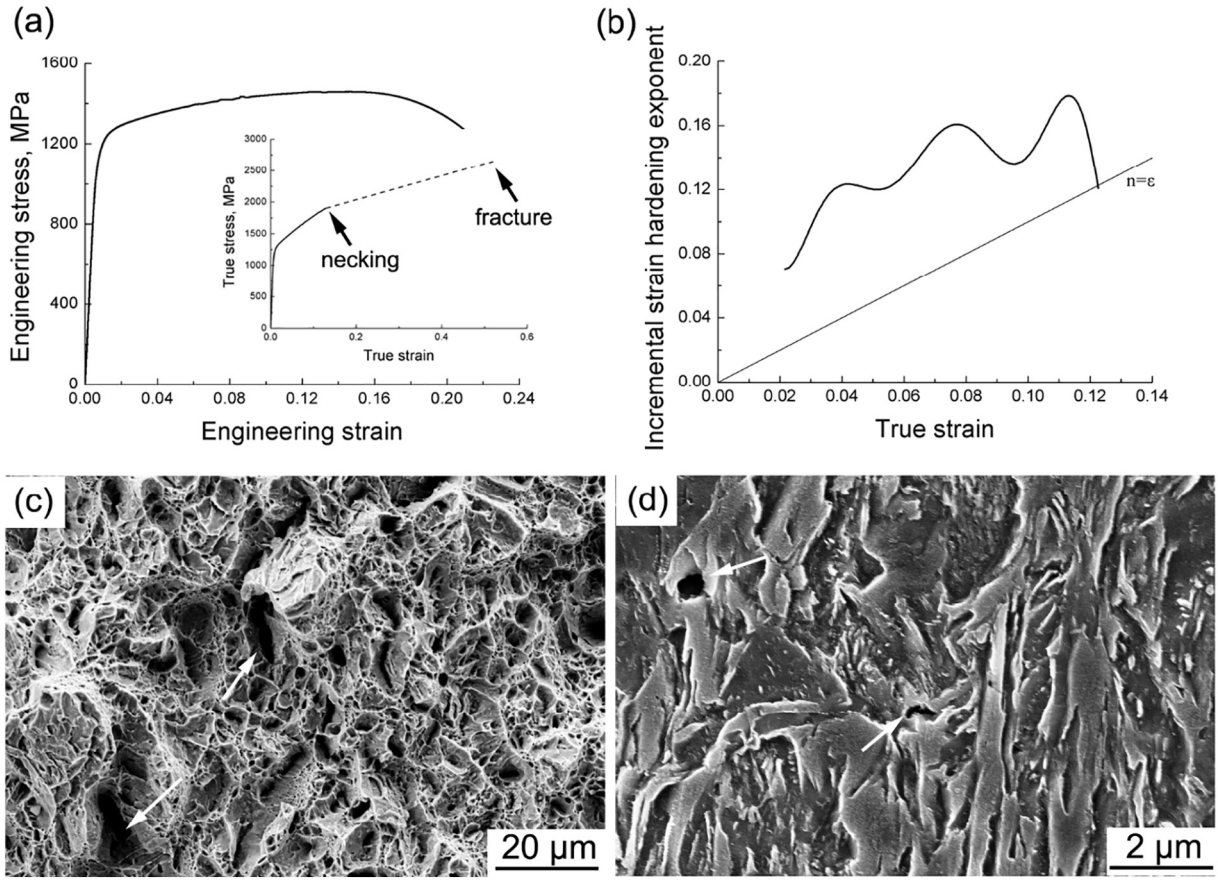

Fig. 1. (a) Engineering and true stress-strain curves and (b) incremental strain hardening exponent; (c) SEM micrograph of the fracture surface and (d) microstructure adjacent to the tensile fracture surface on cross section.

grades using interrupted tensile tests correlated with EBSD [2] and X-ray diffraction [3]), a high and sustainable strain hardening exponent is obtained, leading to a large uniform elongation of 14.1 ± 0.65% and a total elongation of 20.7 ± 0.30%. The high yield strength (1138 ± 21 MPa) and ultimate tensile strength (1452 ± 6 MPa) originate from the martensitic matrix embedded with fresh martensite formed during straining. The product of tensile strength and total elongation is equal to ~30,000 MPa·%, which is large in comparison with typical values 15,000–20,000 MPa·% in the case of ferrite-martensite dual phase steels [13] and transformation-induced plasticity steels [14] of first generation AHSSs. Generally, it is believed that this large product indicates a high fracture toughness [15]. Fig. 1(c) corresponds to a representative micrograph of the fracture surface. It consists of many small dimples and several deep cracks, indicating a ductile fracture mechanism. These dimples dominantly originate from the interfaces between RA (namely fresh martensite after transformation) and tempered martensite as indicated by arrows in Fig. 1(d). It is mainly due to the large difference in strength between them, which is reminiscent of the void nucleation at the interface between ferrite and martensite observed in a ferrite-martensite dual phase steel [16].

DENT specimens with initial cracks produced by fresh razor blade have been deformed in tension. The load-displacement curve is given in Fig. 2(a). The curve exhibits a sharp load drop. From the crack initiation starting at the load indicated by the arrow in Fig. 2(a), intergranular brittle fracture occurs, as shown in Fig. 2(b). Typical intergranular facets are dominant with very few dimples (indicated by white arrows). In addition, some transverse cracks are also observed. In order to elucidate the fracture mechanism, the loading of a DENT specimen was interrupted just before the maximum load. A part of the specimen was cut, mounted, polished to mid-thickness and etched. As shown in Fig. 2(c), the overall crack path is somewhat straight. Fig. 2(d) shows the microstructure near the tip of the crack. The solid and dashed lines illustrate the boundaries of martensitic packets. The dashed lines also indicate the crack path. This shows that the crack mainly propagates along the martensitic packet boundaries. The region of black lines is enlarged in Fig. 2(e), where crack propagates along the interfaces between film RA and tempered martensitic laths. The white arrows point out blocky RA islands along the crack path. In a word, the crack dominantly propagates along the boundaries of the martensitic packets (where blocky RA distributes) and occasionally along the film RA oriented parallel to the direction of crack propagation.

This study thus shows that ductile fracture occurs in uniaxial tension while intergranular brittle fracture occurs with DENT specimen of the same Q & P steel. This change of fracture mode could be ascribed to the different transformation rates of RA to martensite influenced by the stress triaxiality levels. In uniaxial tension, due to the small stress triaxiality, the true stress slowly increases with increasing true strain (Fig. 1(a)). It leads to a gradual RA-to-martensite transformation [2,3,17] and the volume fraction of RA decreases from 18.2% to 4.9% at uniform elongation (the start of necking). This brings a large work hardening ability (Fig. 1(b)) and in turn a large uniform elongation of 14.1 ± 0.65% (corresponding to a true strain of 0.13 ± 0.01), indicating a good resistance to necking for such high level of strength. By tempering at 200 °C for 2 h, the microstructure at uniform elongation (Fig. 3(a)) reveals that large blocky and large film RA grains have transformed to martensite and small RA grains still keep untransformed. Dislocation density in the tempered martensite increases during deformation, which can reduce the strength difference between tempered and fresh martensite, resulting in more homogenous stress partitioning between them after necking. This can help to prevent the brittle intergranular

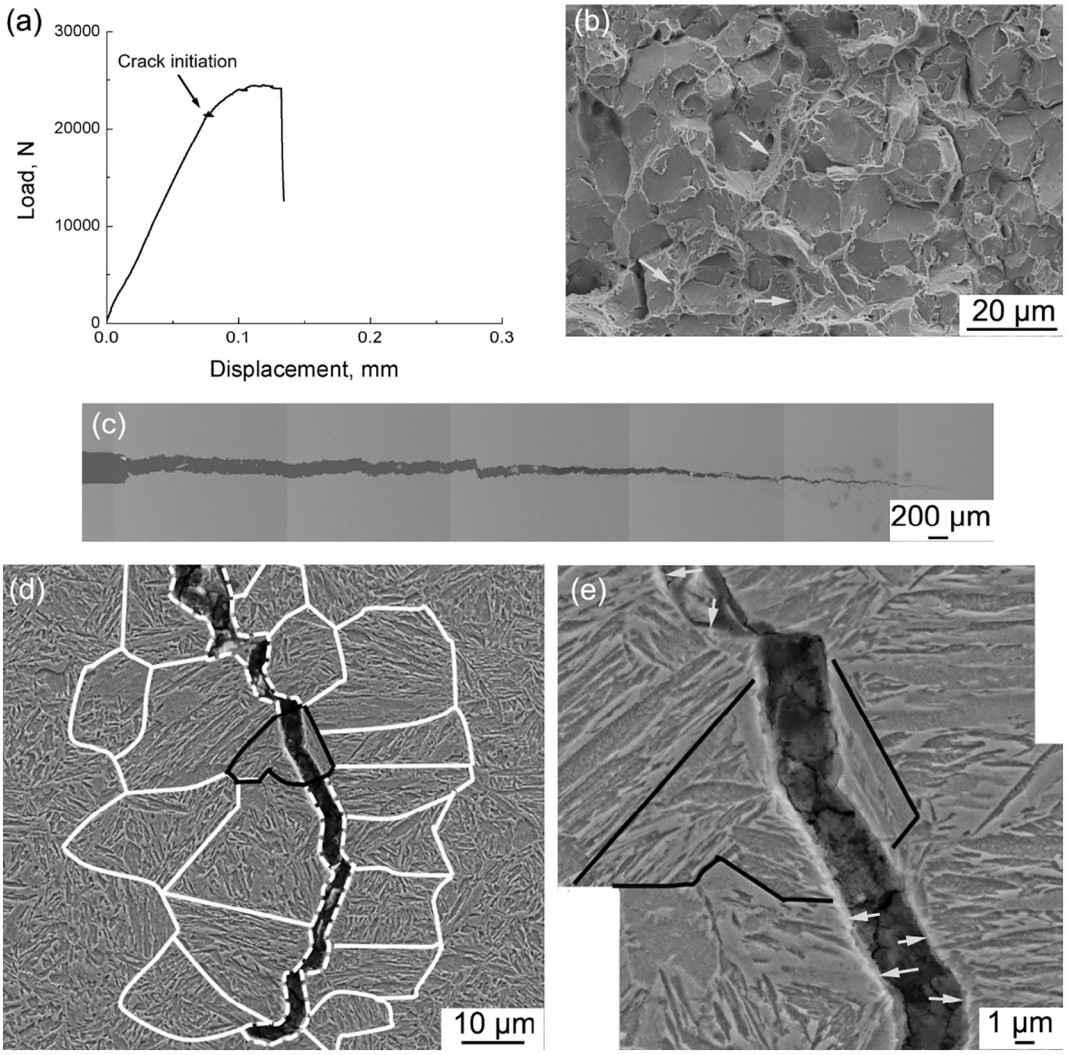

Fig. 2. (a) Load-displacement curve of a DENT specimen and (b) SEM micrograph of the fracture surface where white arrows point out the dimples. (c) Stable crack propagation observed by stopping a DENT test just before the maximum load and (d) the corresponding microstructure at the tip of this crack (solid and dashed lines illustrate martensitic packet boundaries while dashed lines also indicate the crack path); (e) enlargement of black line area in (d) where white arrows indicate the blocky retained austenite.

fracture. On the other hand, previous study on the same Q & P steel has shown that strain partitioning during plastic deformation results in strain localization between tempered and fresh martensite (transformed from RA), leading to void nucleation and growth at their interfaces during necking [4]. Therefore, the voids predominantly nucleate at the interfaces between fresh and tempered martensite, which is also observed in Fig. 1(d). This process is sketched in Fig. 3(c). Some cracks also form as shown in Fig. 1(c). However, their propagation is inhibited predominantly because of large deformation around them in terms of dislocation motion resistance [18]. Landron et al. has demonstrated that increasing strain after a critical value can dramatically increase the number of void nucleation in ferrite-martensite dual phase steel [19]. In present study, with an increase in the strain after necking, the void nucleation can be also accelerated and the continuous transformation of 4.9% RA to martensite further provides new sites for void nucleation, finally leading to the ductile fracture.

In contrast, higher stress triaxiality in the DENT specimen results in a faster transformation rate of RA-to-martensite in the near crack tip region [20]. This allows that RA grains adjacent to the crack tip quickly and almost fully transform to martensite as shown in Fig. 3(b) within a small true strain of ~6%. Similar phenomenon has been reported in TRIP-assisted multi-phase steel [10]. It is important to indicate here that tiny film RA might not have been detected. This almost full transformation region is about ~60 μm from the crack tip, which contains about six martensitic packets. As a result, fresh martensite, transformed from blocky RA islands dispersed along the boundaries of martensitic packets, forms a brittle necklace. This is sketched in Fig. 3(d). In addition, the stress triaxiality is further enhanced by the formation of hard fresh martensite. Because of this high stress triaxiality and, in turn, high maximum principle stress in front of the crack tip [21], microcracks nucleate at the interfaces between fresh and tempered martensite, and predominantly propagate along this brittle necklace, and occasionally propagate along the film RA (such as observed in Fig. 2(d, e)). When the crack progressively propagates, the RA grains next to the crack tip continuously transform to martensite. This leads to a stable, though quite brittle, crack propagation. The equivalent circled diameter of the facets is equal to 10.9 ± 3.8 μm (Fig. 2(b)), which is similar to 10.8 ± 3.9 μm of martensitic packets (Fig. 2(d)). Again, this supports that the brittle fracture mainly occurs along the martensitic packet boundaries.

In conclusion, ductile and brittle fractures are observed using uniaxial tension and DENT tests in a two-step Q & P steel, respectively. In uniaxial tension, a large volume fraction of RA ensures a continuous transformation of RA-to-martensite because of small stress triaxiality, resulting in a large ductility, with voids nucleating at the interfaces between fresh and tempered martensite, leading finally to a ductile

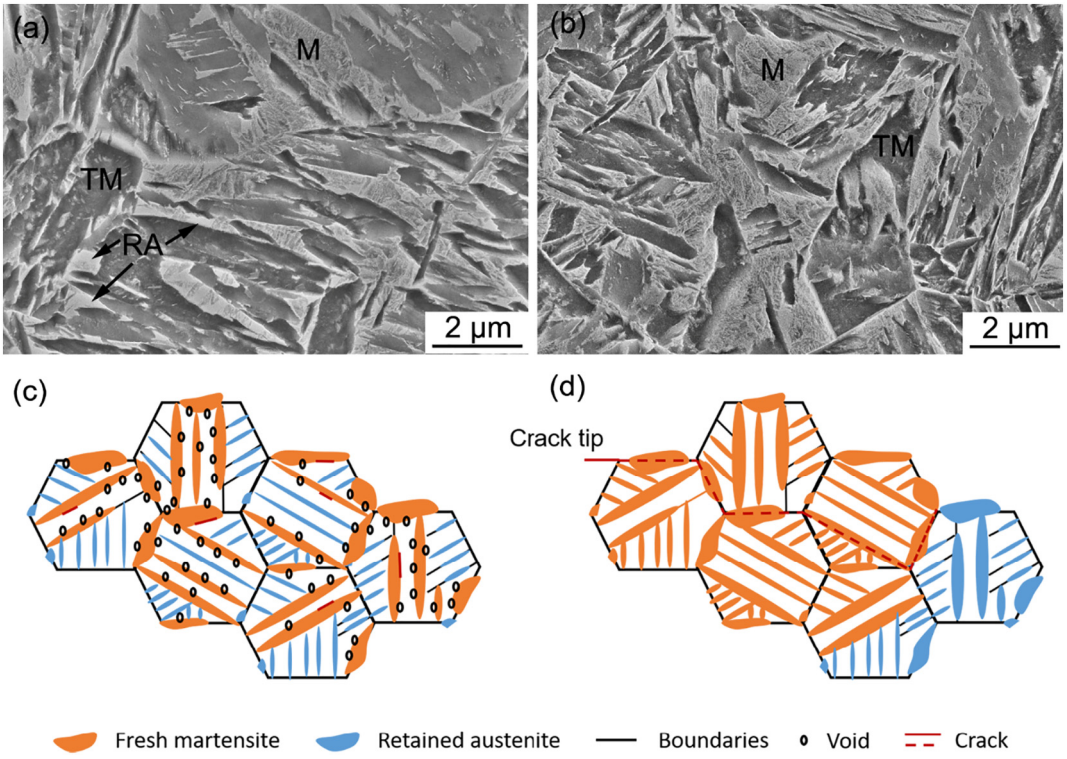

Fig. 3. (a, b) Microstructures of (a) uniaxial tension specimen at uniform elongation and (b) DENT specimen in the front of the crack tip after tempering at 200 °C for 2 h in order to show the fresh martensite transformed from retained austenite. (c, d) Schematic illustration of fracture mechanisms in (c) uniaxial tension specimen and (d) DENT specimen. *M* stands for fresh martensite, *TM* for tempered martensite and *RA* for retained austenite.

fracture mechanism. Whereas during DENT test, large stress triaxiality near the crack tip region quickly promotes the transformation of RA to martensite and in turn the formation of fresh martensite brittle necklace along the boundaries of martensitic packets at small deformation. Additionally because of high maximum principle stress, crack initiates and propagates along this brittle necklace, leading to brittle fracture. Thus, the balance between resistance to plastic localization and resistance to cracking requires a control of the RA-to-martensite transformation rate through the adjustment of the amount and morphology of RA in this studied Q & P steel.

Acknowledgements

This work was funded by ArcelorMittal Global R&D Maizières Products (C.2015.0105) in France.

References

[1] J. Speer, D. Matlock, B. de Cooman, J. Schroth, Acta Mater. 51 (2003) 2611–2622.
[2] D. de Knijf, C. Föjer, L.A.I. Kestens, R. Petrov, Mater. Sci. Eng. A 638 (2015) 219–227.
[3] E. de Moor, S. Lacroix, A.J. Clarke, J. Penning, J.G. Speer, Metall. Mater. Trans. A 39 (2008) 2586–2595.
[4] M.M. Wang, J.C. Hell, C.C. Tasan, Scr. Mater. 138 (2017) 1–5.
[5] M. Santofimia, L. Zhao, R. Petrov, C. Kwakernaak, W. Sloof, J. Sietsma, Acta Mater. 59 (2011) 6059–6068.
[6] E. de Moor, J.G. Speer, D.K. Matlock, J.-H. Kwak, S.-B. Lee, ISIJ Int. 51 (2011) 137–144.
[7] D.P. Koistinen, R.E. Marburger, Acta Metall. 7 (1959) 59–60.
[8] D. Casellas, A. Lara, D. Frómeta, D. Gutiérrez, S. Molas, L. Pérez, J. Rehrl, C. Suppan, Metall. Mater. Trans. A 48 (2017) 86–94.
[9] F. Hisker, R. Thiessen, T. Heller, Mater. Sci. Forum 706–709 (2012) 925–930.
[10] G. Lacroix, T. Pardoen, P.J. Jacques, Acta Mater. 56 (2008) 3900–3913.
[11] S. Allain, G. Geandier, J.C. Hell, M. Soler, F. Danoix, M. Gouné, Scr. Mater. 131 (2017) 15–18.
[12] E. Girault, P. Jacques, P. Harlet, K. Mols, J. van Humbeeck, E. Aernoudt, F. Delannay, Mater. Charact. 40 (1998) 111–118.
[13] Z.P. Xiong, A.A. Saleh, A.G. Kostryzhev, E.V. Pereloma, J. Alloys Compd. 721 (2017) 291–306.
[14] Z.P. Xiong, A.G. Kostryzhev, A.A. Saleh, L. Chen, E.V. Pereloma, Mater. Sci. Eng. A 664 (2016) 26–42.
[15] Y. Rong, Int. Heat Treat. Surf. Eng. 5 (2011) 145–154.
[16] N. Saeidi, F. Ashrafizadeh, B. Niroumand, M.R. Forouzan, F. Barlat, Eng. Fract. Mech. 127 (2014) 97–103.
[17] P. Jacques, Q. Furnémont, F. Lani, T. Pardoen, F. Delannay, Acta Mater. 55 (2007) 3681–3693.
[18] K. Habib, M. Koyama, T. Tsuchiyama, H. Noguchi, Mater. Res. Lett. 6 (2018) 61–66.
[19] C. Landron, O. Bouaziz, E. Maire, J. Adrien, Scr. Mater. 63 (2010) 973–976.
[20] P. Jacques, Q. Furnémont, T. Pardoen, F. Delannay, Acta Mater. 49 (2001) 139–152.
[21] A. Pineau, A.A. Benzerga, T. Pardoen, Acta Mater. 107 (2016) 424–483.